Supplementary Material

1 Details on Surfactant Measurements

We conducted a brief pre-study, in which we compared the surface activity of sea water samples before and after storage at + 4°C, - 20°C and - 80°C to decide, which freezing temperature was the best suitable option. Samples were collected in the Kiel Bight on the 11th of December 2017. On the day of sampling (t_0), samples were stored in falcon tubes without any pre-treatment and immediately frozen. On day t_0, we measured in total three, fresh samples and repeated the measurement on the second day (t_2) for all storage options. In **Figure S1**, the change of surface activity in respect to the fresh samples measured at day t_0, is compared. The storage at - 80°C reproduced the most reliable measurements. Conclusively, we decided to store the samples at - 80°C and thus followed the option Salter et al. (2011) had chosen for their Atlantic seawater samples, also intended for later on lab-based analysis of surface activity.

We are aware of the possibility that longer storage times may have influenced surface activity further, although no change occurred within the first two days. Schneider-Zapp et al. (2013) tested several storage options for riverine and estuarian SML samples over four weeks. They compared seven different storage protocols and the change over time of several parameters, among others surface activity, to the untreated sample (stored at + 4°C). They concluded that none of the protocols performed better than the untreated sample storage when taking into account all parameters tested. For surface activity, however, no significant change over storage time occurred for the frozen, filtered samples (- 20°C) and the untreated samples (+ 4°C) likewise.

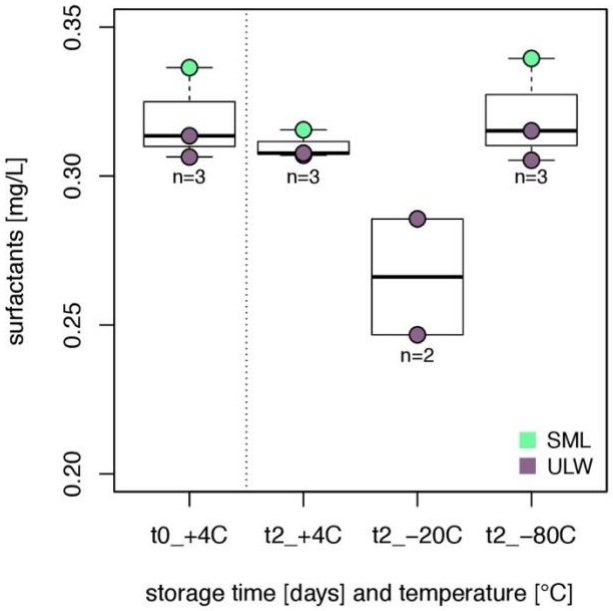

Figure S1. Comparison of storage temperatures (+4°C, -20°C, -80°C) of SML and ULW samples for the analysis of surface activity by phase sensitive alternating voltammetry over the range of two days (t0, t2).

Table S1. Summary of Calibration and Precision Details for Voltammetric Measurements.

Stations	**Precision**	**Calibration line**	R^2	***N***
	[mg TX-100 equiv. L^{-1}]			
1 to 3	±0.019	y = 662x + 8	0.9534	4
4 to 14	±0.010	y = 622x + 2	0.9996	9
15 to 19	±0.021	y = 670x − 8	0.9967	5
Explanation: *Precision of measurements is expressed as the relative standard deviation around the sample mean of 0.2 mg TX-100 equiv. L^{-1}, and was calculated using the standard deviation from targeted TX-100 concentrations. N describes the number of different concentrations used to derive the calibration line.*				

2 Difference in Salinity Across the Filament's Front

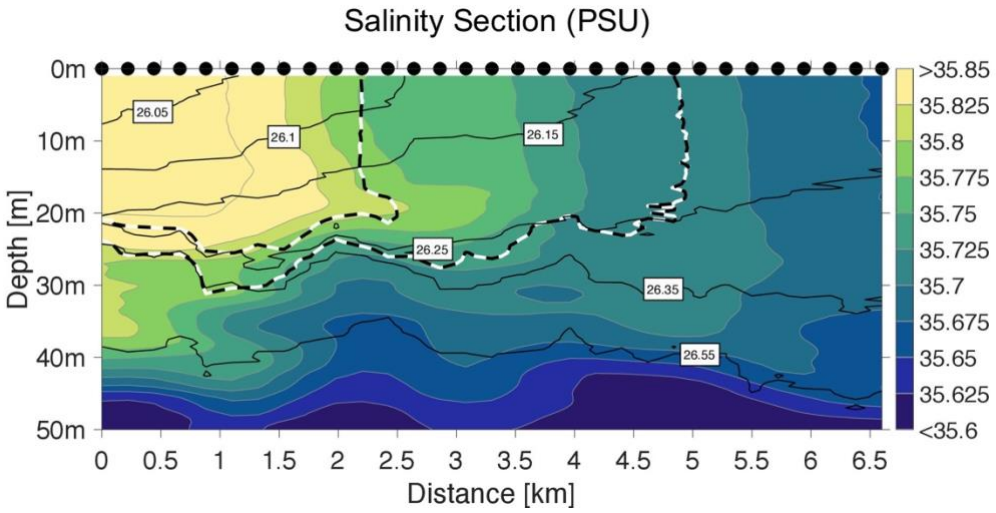

Figure S2. The salinity cross section against depth was performed on 2 February 2018. It revealed a clear separation between less saline, upwelling water masses inside (≤35.71) and saltier, stratified waters (≥35.76) outside the filament. The complementary temperature section is depicted in the main article in Figure 2D. The temperature threshold for stations sampled inside and outside the filament is superimposed in dashed black/white lines. The black lines indicate density layers. Black dots mark the actual position where the microstructure has been deployed.

3 Differences in Organic Matter and Neuston Composition Across the Filament's Front

Table S2. Differences across the filaments front split into subgroups of depths and as presented in Figure 3 in the main text.

	Concentration				**Test statistics**	
					Differences	
Included data	**SML** (n=19)		**ULW** (n=19)		**SML**	**ULW**
	Inside (n=12)	**Outside** (n=7)	**Inside** (n=12)	**Outside** (n=7)	**Inside vs. Outside**	
	[Mean ±SD]		[Mean ±SD]		[*p*-value <]	
TOC [µM]	93.9 ±13.2	86.0 ±5.4	81.6 ±8.1	73.7 ±6.0	0.045 *	0.036 *
TN [µM]	25.9 ±3.3	21.6 ±2.0	23.8 ±2.2	19.4 ±0.7	0.013 *	0.001 ***
TAA [µM]	1.86 ±0.47	1.49 ±0.29	1.39 ±0.42	0.91 ±0.14	0.142	0.006 **
residual **TCHO** [nM]	488 ±68	484 ±55	435 ±74	412 ±44	0.967	0.651
Glucose [nM]	892 ±577	371 ±207	718 ±481	236 ±128	0.045 *	0.010 **
SA [mg TX-100 equiv. L^{-1}]	0.28 ±0.11	0.22 ±0.18	0.22 ±0.12	0.16 ±0.07	0.138	0.330
Chlorophyll *a* [mg m^{-3}]$_b$	NA	NA	1.79 ±0.45	1.21 ±0.45	NA	0.010 **
pico-**CBL** [10^3 cells mL^{-1}]	4.4 ±2.0	57 ±42	5.0 ±2.5	41 ±36	0.001 ***	0.003 **
nano-**CBL** [10^3 cells mL^{-1}]	0.98 ±0.28	1.49 ±0.38	1.28 ±0.32	1.41 ±0.76	0.010 **	0.968
pico-**NCBL** [10^3 cells mL^{-1}]	38±17	51 ±14	37 ±18	38 ±17	0.101	0.968
nano-**NCBL** [10^3 cells mL^{-1}]	5.8 ±2.6	6.0 ±2.3	10.8 ±5.1	5.7 ±2.9	0.774	0.029 *
LNA [10^6 cells mL^{-1}]	0.62 ±0.24	1.10 ±0.30	0.54 ±0.26	0.81 ±0.36	0.002 **	0.101

HNA [10^6 cells mL^{-1}]	1.39 ±0.45	1.30 ±0.21	1.44 ±0.59	1.12 ±0.34	0.773	0.340

Abbreviations*: Sea surface microlayer (SML), underlying water (ULW), standard deviation (SD), total organic carbon (TOC), total nitrogen (TN), total amino acids (TAA), total combined carbohydrates (TCHO), surfactant concentration (SA), cyanobacteria-like phytoplankton cells (CBL), non-cyanobacteria-like phytoplankton cells (NCBL), low nucleic acid content bacteria (LNA), high nucleic acid content bacteria (HNA).*

Explanation: *This table presents mean concentrations and standard deviations as measured within the four subgroups. Test statistics refer to differences obtained for the SML and ULW between the inside and outside of the filament, respectively. Differences were calculated using the* Mann Whitney *U*-test*. Significances are expressed in* p*-values. Significance levels are expressed in asterisks, with * being equivalent to a significance level of* $p < 0.05$*, ** of* $p < 0.01$*and *** of* $p < 0.001$*.* [b] *MODIS-aqua satellite-derived Chl a concentration, averaged over one day and 1km² area (data as provided by NASA).*

4 Morning Stations Manifest Cross-Frontal Differences in the SML

We assessed if i) sampling dates due to changing meteorological conditions or ii) diurnal variation could have caused the observed sub-mesoscale differences in the SML.

i) In the main work, the focus of the analysis was set on difference in SML characteristics occurring across the hydrological front of a filament. Sampling on both sides of the filament occurred within 12 days, however not in a reciprocal manner. This is due to the dynamic front which progressed in time and space and could not be sufficiently resolved by satellite imaging. For orientation, the filament's front was marked by a drifter buoy; However, fine-scale variability altered the buoys relative distance to the front. It was already ruled out that results were biased by divergent meteorological conditions, which may have coincided with the different sampling dates of the filament's sides. As surfactants and TOC measurement are central to this work, we would further like to exclude that these variables corresponded to solar irradiance or wind speed. Surfactant concentration in the SML and ULW were not related to solar radiation (Spearman Rank correlation test; SML: *p*-value > 0.682, n=19 and ULW: *p*-value > 0.204, n=19). Also, wind speed did neither affect absolute surfactant concentration in the SML (*p*-value > 0.488, n=19) nor EF_{surf} (*p*-value > 0.863, N=19). For TOC concentration and enrichment, correlations yielded likewise insignificant results.

ii) In the main results, morning and afternoon stations have been integrated. This could lead to a potential bias as it is known that diurnal variations in biology may influence organic matter composition and microorganisms (Stolle et al., 2020). It was therefore investigated whether samples obtained in the morning exhibited the same sub-mesoscale differences across the filament's front as concluded in the main work. By referring to the morning samples only, the influence of the sun i.e. the diel radiation history on samples is reduced to a minimum. In the morning, four stations were sampled inside and five stations were acquired outside the filament. The data for the morning stations including absolute concentrations and EFs is presented in **Table S3**. In summary, it was previously shown that concentration of organic matter was reduced, the enrichment factors were in general larger and neuston organisms preferentially colonized the SML outside the filament. For instance, TOC concentration in the SML was affected by the influence of regimes as a mean TOC concentration of 90.5 ±11.8 µM and 84.7 ±4.8 µM was measured inside and outside, respectively. In accordance to the main findings, this was manifested by the even greater difference observed inside and outside the filament for ULW TOC concentration (84.1 ±11.9 µM and 73.5 ±7.0 µM). This pattern applied to all organic matter classes

although it was less pronounced for surfactant concentrations. Enrichment factors outside the filament exceeded the EFs observed inside the filament which is again in compliance with the conclusions drawn in the main article. For instance, in the morning EF_{TAA} was 1.3 ±0.4 inside in comparison to 1.6 ±0.4 outside the filament. The comparison of morning stations showed likewise that organisms colonized preferentially the SML outside the filament and were depleted inside with regards to nano-phytoplankton cells. For example, pico-NCBL cells were enriched by 1.0 ±0.2 inside in comparison to an $EF_{pico\text{-}NCBL}$ of 1.3 ±0.3 outside the filament. Conclusively, we are convinced that the observed sub-mesoscale differences of the SML across the filaments front were not biased by our sampling strategy but controlled by underlying hydrology. It thus contributes to the understanding of complex and often enigmatic SML dynamics.

Table S3. Differences across the filaments front split into subgroups of depths and as sampled at the morning stations.

Morning Stations	**Concentration**				**EFs**	
Included data	**SML** (n=9)		**ULW** (n=9)		**inside**	**outside**
	Inside (n=4)	**Outside** (n=5)	**Inside** (n=4)	**Outside** (n=5)		
	[Mean ±SD]		[Mean ±SD]		[Mean ±SD]	
TOC [µM]	90.5 ±11.8	84.7 ±4.8	84.1 ±11.9	73.5 ±7.0	1.1 ±0.1	1.2 ±0.1
TN [µM]	24.3 ±2.7	21.5 ±2.5	24.2 ±2.6	19.5 ±0.75	1.0 ±0.1	1.1 ±0.1
TAA [µM]	1.58 ±0.29	1.44 ±0.34	1.28 ±0.44	0.94 ±0.15	1.3 ±0.4	1.6 ±0.4
residual **TCHO** [nM]	483 ±86	461 ±46	440 ±67	401 ±44	1.1 ±0.1	1.2 ±0.1
Glucose [nM]	266 ±39	257 ±59	278 ±86	172 ±55	1.0 ±0.4	1.6 ±0.5
SA [mg TX-100 equiv. L^{-1}]	0.26 ±0.15	0.19 ±0.16	0.24 ±0.17	0.16 ±0.07	1.2 ±0.3	1.1 ±0.4
pico-**CBL** [10^3 cells mL^{-1}]	5.9 ±2.1	54 ±38	6.3 ±2.1	48 ±40	1.0 ±0.4	1.4 ±0.5
nano-**CBL** [10^3 cells mL^{-1}]	0.93 ±0.30	1.56 ±0.40	1.26 ±0.36	1.70 ±0.70	0.8 ±0.2	1.0 ±0.2

pico-**NCBL** [10^3 cells mL^{-1}]	45 ±15	54 ±13	45 ±11	44 ±15	1.0 ±0.2	1.3 ±0.3
nano-**NCBL** [10^3 cells mL^{-1}]	4.2 ±1.4	5.0 ±1.6	7.8 ±3.1	6.1 ±3.2	0.6 ±0.4	0.9 ±0.3
LNA [10^6 cells mL^{-1}]	0.74 ±0.22	1.14 ±0.34	0.58 ±0.27	0.92 ±0.36	1.4 ±0.4	1.3 ±0.1
HNA [10^6 cells mL^{-1}]	1.53 ±0.33	1.35 ±0.23	1.51 ±0.50	1.25 ±0.30	1.1 ±0.2	1.1 ±0.1

Abbreviations*: SML Sea surface microlayer (SML), underlying water (ULW), mean (M), standard deviation (SD), enrichment factor (EF), total organic carbon (TOC), total nitrogen (TN), total amino acids (TAA), total combined carbohydrates (TCHO), surfactant concentration (SA), cyanobacteria-like phytoplankton cells (CBL), non-cyanobacteria-like phytoplankton cells (NCBL), low nucleic acid content bacteria (LNA), high nucleic acid content bacteria (HNA).*

Explanation: *This table presents mean concentrations and standard deviations as measured for morning stations divided in the four subgroups. Test statistics refer to differences obtained for the SML and ULW between the inside and outside of the filament, respectively. Enrichment factors were calculated by dividing the SML concentration of substances/ organisms by the respective concentration of the ULW.*

5 Principal Component Analysis of TAA and TCHO (PC3)

When conducting a PCA, variance occurring in the data of the molecular composition of TAA and TCHO respectively is congregated onto principal components (PC). Although the first and second PC explain the highest portion of variance in the data, there is still further hidden variance in subsequent PC. We depicted also the third PC (PC3) of TAA and TCHO since we considered this supplementary information valuable to justify our conclusions that the SML is molecularly distinct from the ULW, even though sampled on different sides of the filament front.

In the PCA derived from amino acid composition, PC2 pictures the already discussed distinct composition of the SML (PC2 explains 24.8% of the variance). PC3 explains an additional 9.3% of variance which is again owed, at least in parts, to the divergent behavior of the SML (**Figure S3A**). Likewise, PC3 in the residual TCHO revealed differences between the molecular SML and ULW composition explaining in total 14.3% of the variance. In particular Galactose and, to a smaller extend, Guluronic acid are characteristic for the SML, while the opposing carbohydrates in the ULW are Mannose and Xylose (**Figure S3B**).

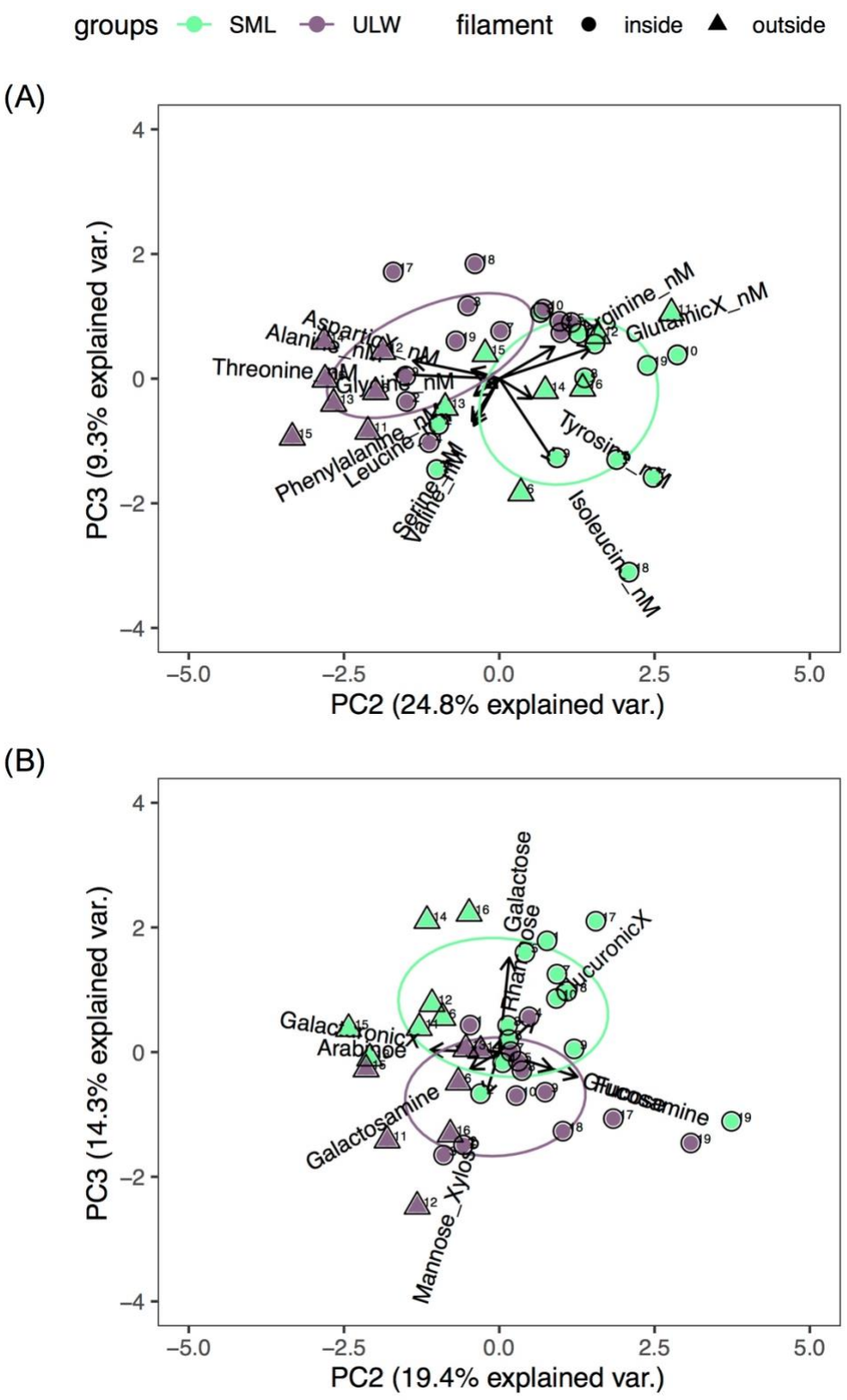

Figure S3. Principal Component Analysis (PCA) depicting the second and third Principal Components (PC2 and PC3) of **(A)** total amino acid (TAA) and **(B)** total combined carbohydrates (TCHO) composition. Arrows indicate the relative molar contribution of TAA and TCHO. SML and ULW are represented by green and grey, respectively. Circles and triangles represent the hydrological regime i.e. inside and outside the filament.

6 Supplementary Information on Degradation Indices

Following the protocol of Dauwe and Middelburg (1998) and Dauwe et al. (1999), degradation indices (DI) were derived from the PCA of TAA. PC1 reflects the greatest variance in TAA composition, which directly translates into the alteration of organic matter. The PC1 axis of TAA in this study was defined by a bundle of amino acids often associated to fresh production, including Leucine and Phenylalanine, on one side and by amino acids associated to degraded organic matter, as represented by Serine and Glycine, on the other side (Dauwe and Middelburg, 1998; Amon et al., 2001; Davis et al., 2009). DI are suggested to serve as the best indicator of intermediate degradation stages. In contrast, the amount of nitrogen and organic carbon incorporated into TAA relative to TN and TOC can be used to derive the most reliable assumption during early degradation stages (Davis et al., 2009). Indices are derived independently from another.

The amount of nitrogen and organic carbon incorporated into amino acids ($[THAA]_i \times \sum_i C_i$) relative to TN and TOC concentration (*TAA-N/ OC yield [%]*) (Equation 1) was used to derive the second, and independent of the first, degradation index (Davis et al., 2009).

$$TAA\ C\ yield = \frac{[TAA]_i \times \sum_i C_i}{[TOC]} \times 100 \quad (1)$$

TAA-N /OC yields obtained for the ULW only indicated slight difference across the filaments front (Inside: 9.6 ±3.5/ 7.8 ±2.2%, n=9; Outside: 6.5 ±1.0/ 5.0 ±0.7%, n=7; Mann-Withney *U*-test*;* TAA-N yield: *p*-value> 0.054; TAA-OC yield: *p*-value<0.016). Only minor differences in DI were notable between depths (SML: -0.6 ±2.1; ULW 0.6 ±2.4), while TAA-N/ OC yields differed by 10.3 ±2.7/ 7.8 ±1.6% and 7.8 ±2.9/ 6.3 ±2.1% between the SML and ULW, respectively.

While DI and TAA-N and TAA-OC yields derived from the SML did not show any correlation (**Figure S4A, C**), ULW samples reflected two distinct stages of degradation according to the introduced concept of Davis et al. (2009). ULW samples gathered inside the filament exhibited a drastic change in TAA-OC and TAA-N yields while the range of corresponding DI was comparatively small and values were positive (**Figure S4B, D** circles). The correlation between the DI and TAA-N and TAA-OC yields were significant inside the filament (*Pearson correlation*, TAA-N: r^2=0.71, *p*<0.003, n=9; TAA-OC: r^2=0.62, *p*<0.008, n=9). Outside the filament, ULW samples showed only minor changes in TAA-N and TAA-OC yields but differed over a broader range in their DI (**Figure S4B, D** triangles). The correlation between the DI and TAA yields were also significant (*Pearson correlation*, TAA-N: r^2=0.71, *p*<0.011, n=7; TAA-OC: r^2=0.88, *p*<0.002, n=7).

The last three stations sampled inside the filament were considered outliers and thus excluded from the correlations. Stations 17 to 19 were characterized by DI and TAA yields, which are representative for a most advanced state of diagenesis. Initially, these stations were assigned to belong to the upwelling filament because water temperatures were among the coldest measured along the cruise track. The unexpected profiles derived from the molecular TAA composition regarding their diagenetic state could be explained by the premise that the coldest water masses upwelled only most recently and primary production has not yet proceeded. Concurrently, the PCA of residual TCHO suggested that stations 17 to 19 were closely affiliated to all other stations sampled inside the filament. However, these stations were further characterized by Fuc. The rise in phytoplankton abundance has been connected to a brief increase of the molar fraction of Fuc (Guimarães et al., 2013). This suggests that a phytoplankton bloom almost started, but did not alter TAA yet.

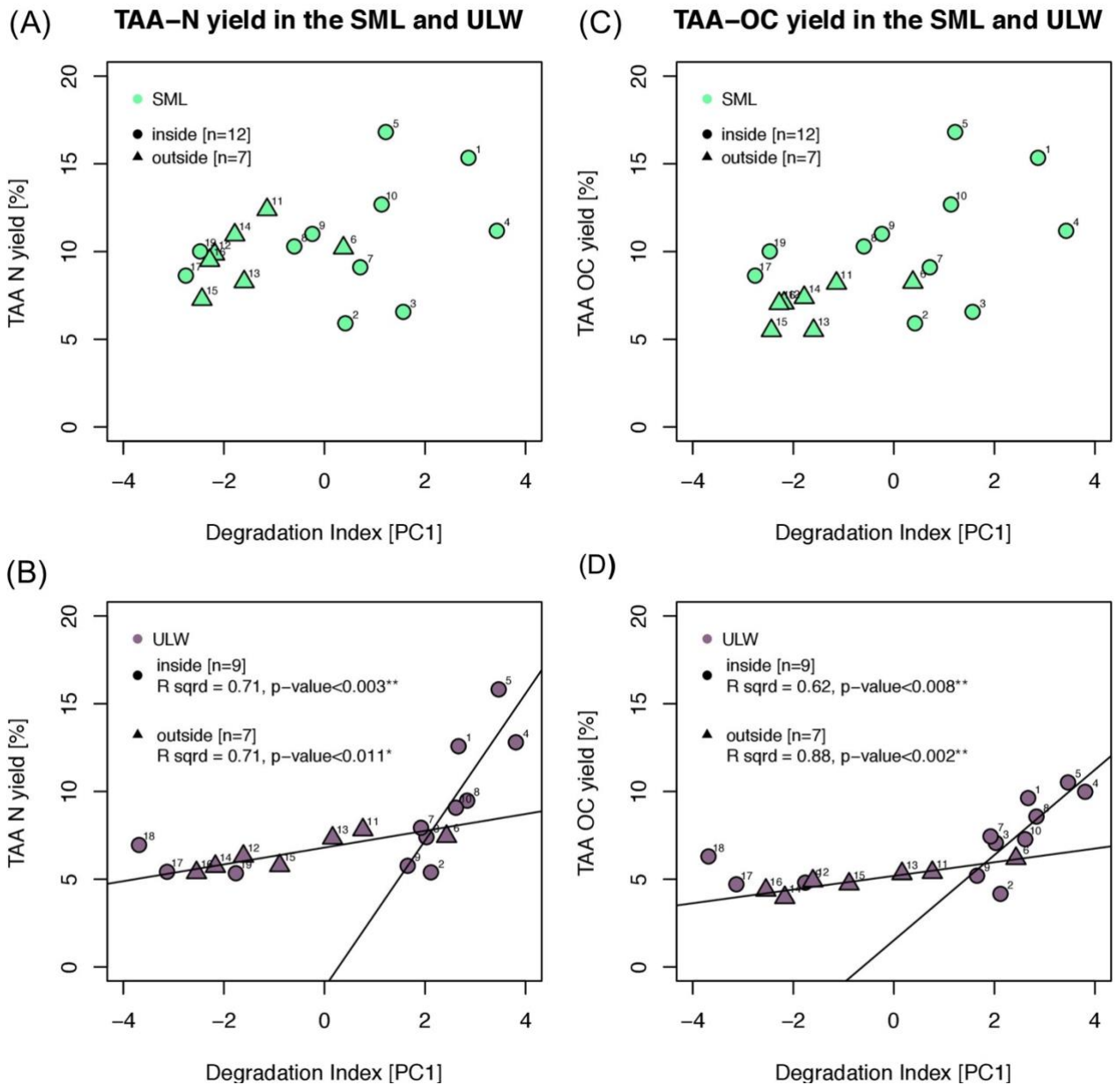

Figure S4. Degradation indices (DI) and TAA nitrogen and organic carbon yields (TAA-N and TAA-OC yields) inside and outside the filament, respectively marked as circles and triangles. **(A)** Relationship of TAA-N yields and independently derived DI from the first Principal Component (PC) of the Principal Components Analysis (PCA) in the SML. **(B)** Relationship of TAA-N yields and independently derived DI from the first PC in the ULW. Across the filament edge, significantly different correlations reflected divergent states of degradation. **(C)** Relationship of TAA-OC yields and independently derived DI from the first PC in the SML. **(D)** Relationship of TAA-OC yields and independently derived DI from the first PC in the ULW. Across the filament edge, significantly different correlations reflected divergent states of degradation.

References

Amon, Rainer M.W., Hans Peter Fitznar, and Ronald Benner. 2001. “Linkages among the Bioreactivity, Chemical Composition, and Diagenetic State of Marine Dissolved Organic Matter.” *Limnology and Oceanography* 46 (2): 287–97. https://doi.org/10.4319/lo.2001.46.2.0287.

Dauwe, B., J. J. Middelburg, P. M.J. Herman, and C. H.R. Heip. 1999. “Linking Diagenetic Alteration of Amino Acids and Bulk Organic Matter Reactivity.” *Limnology and Oceanography* 44 (7): 1809–14. https://doi.org/10.4319/lo.1999.44.7.1809.

Dauwe, Birgit, and Jack J. Middelburg. 1998. “Amino Acids and Hexosamines as Indicators of Organic Matter Degradation State in North Sea Sediments.” *Limnology and Oceanography* 43 (5): 782–98. https://doi.org/10.4319/lo.1998.43.5.0782.

Davis, Jenny, Karl Kaiser, and Ronald Benner. 2009. “Amino Acid and Amino Sugar Yields and Compositions as Indicators of Dissolved Organic Matter Diagenesis.” *Organic Geochemistry* 40 (3): 343–52. https://doi.org/10.1016/j.orggeochem.2008.12.003.

Guimarães, Pablo S., Layanna Zigiotto, Marinês Garcia, Maria J. Dellamano-Oliveira, Armando A.H. Vieira, and Danilo Giroldo. 2013. “Phytoplankton Relationship with Bacterioplankton, Dissolved Carbohydrates and Water Characteristics in a Subtropical Coastal Lagoon.” *Journal of Limnology* 72 (3): 543–54. https://doi.org/10.4081/jlimnol.2013.e45.

Salter, M. E., R. C. Upstill-Goddard, P. D. Nightingale, S. D. Archer, B. Blomquist, D. T. Ho, B. Huebert, P. Schlosser, and M. Yang. 2011. “Impact of an Artificial Surfactant Release on Air-Sea Gas Fluxes during Deep Ocean Gas Exchange Experiment II.” *Journal of Geophysical Research: Oceans* 116 (11): 1–9. https://doi.org/10.1029/2011JC007023.

Schneider-Zapp, K., M. E. Salter, P. J. Mann, and R. C. Upstill-Goddard. 2013. “Technical Note: Comparison of Storage Strategies of Sea Surface Microlayer Samples.” *Biogeosciences* 10 (7): 4927–36. https://doi.org/10.5194/bg-10-4927-2013.

Stolle, Christian, Mariana Ribas-Ribas, Thomas H Badewien, Jonathan Barnes, Lucy J Carpenter, Rosie Chance, Lars Riis Damgaard, et al. 2020. “The MILAN Campaign: Studying Diel Light Effects on the Air–Sea Interface.” *Bulletin of the American Meteorological Society* 101 (2): E146–66. https://doi.org/10.1175/BAMS-D-17-0329.1.